Differences in the resistive and thermodynamic properties of the single crystalline chiral superconductor candidate SrPtAs

Ashley Weiland, Frederico B. Santos, Joe D. Thompson, Eric D. Bauer, Sean M. Thomas, and Priscila F. S. Rosa

MPA-Q, Los Alamos National Laboratory, Los Alamos, New Mexico 87545, USA

The locally noncentrosymmetric superconductor SrPtAs is proposed to host a topological chiral d-wave state, but experimental reports have been limited to polycrystalline samples. Here we report the synthesis of single crystalline SrPtAs grown from Pb flux. SrPtAs crystallizes in the hexagonal space group $P6_3/mmc$ with lattice parameters $a = 4.2445(4)$ Å and $c = 8.9513(18)$ Å. Magnetic susceptibility and electrical resistivity measurements reveal a superconducting transition at $T_c \sim 2.2$ K, in agreement with previous reports on polycrystalline samples. Surprisingly, heat capacity data show only a small bulk transition at 0.7 K. We discuss the possible origins of the discrepancy between the various measurements.

I. INTRODUCTION

SrPtAs, the first hexagonal pnictide-based superconductor [1], is a potential chiral d-wave superconductor due to its hexagonal symmetry and quasi-two-dimensional multiband Fermi surface [2,3]. Chiral superconductors, whose complex superconducting gap function breaks time reversal symmetry (TRS), are of interest due to their nontrivial topology and the potential for quantum computing applications [4]. In non-s-wave pairing, the gap function contains nodes which may be detrimental for superconductivity, but chiral superconducting order parameters may naturally reduce the number of nodes.

In high-symmetry crystal systems, multiple gap functions can be degenerate. For example, in hexagonal systems, $d_{x^2-y^2}$ and d_{xy} superconducting channels are degenerate, and a linear combination of the two results in a chiral $d_{x^2-y^2} \pm id_{xy}$ state. This state would minimize the condensation energy of the superconducting state by avoiding the nodes of pure $d_{x^2-y^2}$ or d_{xy} gaps. Superconductors that contain a high-symmetry crystal structure, strong spin-orbit coupling, magnetic interactions, noncentrosymmetry, TRS breaking, and a quasi-two-dimensional Fermi surface are suitable systems to search for chiral superconductivity. Few known materials are considered candidate chiral superconductors. Examples include Sr_2RuO_4 [5], UPt_3 [6], URu_2Si_2 [7], and potentially SrPtAs [2,8].

SrPtAs crystallizes in the hexagonal nonsymmorphic space group $P6_3/mmc$ (No. 194) [9], wherein Pt and As form a honeycomb lattice. This is in contrast to other pnictide superconductors which form with a square lattice such as LaFePO [10], LaFeAsO [11], LiFeAs [12], NaFeAs [13], and $ThCr_2Si_2$-type structures like $(Ba_{1-x}K_x)Fe_2As_2$ [14]. Although globally centrosymmetric, SrPtAs is locally noncentrosymmetric due to the As-Pt layer breaking inversion symmetry.

Initial measurements, including nuclear magnetic resonance and nuclear quadrupole resonance (NMR/NQR) T_1^{-1} relaxation rates [15], argue that SrPtAs is a conventional s-wave superconductor because the spin-lattice relaxation rate shows a coherence peak and the Knight shift decreases below T_c. Magnetic penetration depth data may be fit to an exponential model and the inferred superfluid density agrees with an isotropic Bardeen-Cooper-Schrieffer (BCS) model [16].

However, muon spin relaxation (μSR) data showing TRS breaking below the superconducting transition temperature T_c, [8] coupled with a recent reevaluation of the NMR data [3], indicate that these data could also correspond to d-wave pairing. Although SrPtAs is the subject of many theoretical investigations discussing band structure topology [17], possible pairing states [18,19], spin orbit coupling [20], topological properties [15], local noncentrosymmetry [21], and gap function symmetry analysis [22], there are very few experimental reports, all of which are limited to polycrystalline samples [1,8,9,15,16]. Several previous works mention the advantages of growing single crystals of SrPtAs to further probe the bulk properties [2,8,15–17,19]. To this end we set out to synthesize and characterize single crystals of SrPtAs.

This work presents the synthesis and physical properties of single crystalline SrPtAs. Although magnetic susceptibility and electrical resistivity measurements reveal superconducting transitions at 2.2 K, specific heat and thermal expansion measurements show a significantly decreased T_c or no T_c, respectively. Herein, we discuss the varying superconducting transition temperatures and draw parallels to MgB_2, another superconductor with a structure derived from AlB_2-like building blocks.

II. METHODS

A. Crystal growth

Crystals of SrPtAs were grown in a Pb flux with a reaction ratio of 1:1:0.7:20 of Sr:Pt:As:Pb. The elements were weighed and placed into an alumina crucible set [23]. The crucibles were placed in a fused-silica tube and flame sealed under vacuum using a hydrogen torch. The reaction vessel was then heated in a programmable furnace to 1150 °C in 72 h, held for 72 h, then cooled to 600 °C at a rate of 3 °C/h. The vessel

was removed from the furnace at 600 °C and inverted into a centrifuge to decant the Pb flux. Reaction ratios of 1:1:1:20 of Sr:Pt:As:Pb following the same heating profile resulted in crystals of nonsuperconducting $SrPt_{0.7}As_{0.9}$ crystallizing in the $P\bar{6}m2$ space group. Single crystals of SrPtAs were kept in an argon glovebox between measurements.

B. Single crystal x-ray diffraction

A single crystal <0.1 mm on each edge was cut from the larger needle used for property measurements and mounted to a CryoLoop using vacuum grease. Data were collected with a Bruker D8 Venture single crystal x-ray diffractometer with an Incoatec IμS microfocus source (Mo radiation $\lambda = 0.71073$ Å) and a PHOTON II CPAD area detector. The raw data frames were processed with the Bruker SAINT software, and a multiscan absorption correction was applied with Bruker SADABS [24]. Starting crystallographic models were obtained in SHELXT [25] using the intrinsic phasing method, and least-squares refinements were performed with SHELXL2018 [26]. The supplementary crystallographic data for this paper can be obtained free of charge from the Cambridge Crystallographic Data Centre [27]. The deposition number for SrPtAs is CSD 2256215.

C. Powder x-ray diffraction

Two single crystals were selected from the same growth batch as the crystal discussed above. The crystals were verified to have the same structure and similar disorder through single crystal x-ray diffraction. The crystals were then ground in methanol and prepared for powder x-ray diffraction through 11-BM's rapid-access mail-in program at the Advanced Photon Source of Argonne National Laboratory.

D. Physical property measurements

Magnetization measurements were obtained through a commercial Quantum Design MPMS SQUID-based magnetometer. Specific heat measurements were made using a commercial Quantum Design PPMS calorimeter that utilizes a quasiadiabatic thermal relaxation technique. The electrical resistivity ρ was characterized using a standard four-probe configuration with an ac resistance bridge. Thermal expansion measurements were performed using a capacitance dilatometer described in Ref. [28] in an adiabatic demagnetization cryostat; ac susceptibility was measured using a set of commercial drive and pickup coils. The ac excitation field was estimated to be 0.042 Oe based on the geometry of the coils.

III. RESULTS AND DISCUSSION

A. Structural characterization

As described in Methods, single crystals of SrPtAs were grown using Pb flux. SrPtAs, of the KZnAs-type derived from the AlB_2 ($P6/mmm$) structure type, crystallizes in the hexagonal space group $P6_3/mmc$ (No. 194) with lattice parameters $a = 4.2445(4)$ Å and $c = 8.9513(18)$ Å, as shown in Fig. 1. In the AlB_2 structure, the B atoms form honeycomb layers separated by Al atoms in the c direction. In contrast, in SrPtAs the B site is occupied by both Pt and As sites,
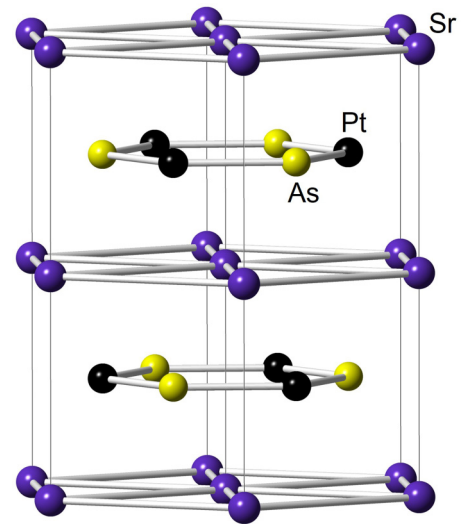

FIG. 1. Crystal structure of SrPtAs ($P6_3/mmc$, No. 194), with Sr in purple, Pt in black, and As in yellow.

which alternate both within the honeycomb lattice and in the c direction such that above each As atom is a Pt atom and above each Pt atom is an As atom. This deviation from the AlB_2 structure results in the doubling of the unit cell along the c axis [9] and breaks local centrosymmetry although the global structure remains centrosymmetric. SrPtAs consists of three crystallographically unique sites, Sr (2*a*), Pt (2*c*), and As (2*d*), where the Pt and As sites are disordered. A more accurate description therefore is $Sr(Pt_{1-x}As_x)(As_{1-y}Pt_y)$ where $x = 0.15(3)$ and $y = 0.116(10)$. Table I shows data collection and refinement parameters, and Table II presents fractional atomic coordinates and displacement parameters. Two single crystals were selected from the same growth batch as the crystal discussed in this paper. The crystals were verified to have the same structure and similar disorder through single crystal x-ray diffraction, then ground and prepared for powder x-ray diffraction. High resolution synchrotron powder x-ray

TABLE I. Crystallographic data, data collection, and refinement parameters of SrPtAs.

Formula	$SrPt_{0.97}As_{1.03}$
Space group	$P6_3/mmc$
a (Å)	4.2445(4)
c (Å)	8.9513(18)
V (Å³)	139.66(4)
Z	2
T (K)	298
θ range (degrees)	4.55–30.40
μ (absorption coefficient, mm⁻¹)	79.37
Measured reflections	6210
Independent reflections	105
$\Delta\rho_{max}$ (largest peak, eÅ⁻³)	2.00
$\Delta\rho_{min}$ (deepest hole, eÅ⁻³)	−2.34
Extinction coefficient	0.031(7)
$R_1(F^2 > 2\sigma(F^2))$	0.029
$wR_2(F^2)$	0.059

TABLE II. Fractional atomic coordinates and anisotropic displacement parameters of SrPtAs.

Site Label	Wyckoff	x	y	z	U_{eq}	Occupancy	U^{11}	U^{22}	U^{33}	U^{12}
Sr1	2a	0	0	0	0.0099(10)	1	0.0091(10)	0.0091(10)	0.0117(13)	0.0045(5)
Pt2/As2	2c	$\frac{1}{3}$	$\frac{2}{3}$	$\frac{1}{4}$	0.0084(4)	0.85(3)/0.15(3)	0.0069(5)	0.0069(5)	0.0114(6)	0.0034(2)
As3/Pt3	2d	$\frac{2}{3}$	$\frac{1}{3}$	$\frac{1}{4}$	0.0100(9)	0.884(10)/0.116(10)	0.0070(10)	0.0070(10)	0.0161(12)	0.0035(5)

diffraction data ($\lambda = 0.459$ Å) were collected under ambient conditions at the 11-BM beamline at the Advanced Photon Source of Argonne National Laboratory. Resulting powder diffraction pattern, shown in Fig. 2, indicates phase composition of SrPtAs > 95% and Pb < 5%.

B. Physical properties

The temperature-dependent magnetic susceptibility (χ) and electrical resistivity (ρ) measurements show a superconducting transition temperature of about 2.2 K, as shown in Figs. 3(a) and 3(b), respectively, consistent with previously reported works on polycrystalline samples of SrPtAs [1]. Transitions visible at 7 K are due to excess elemental Pb that was used as a flux for the crystal growth. The susceptibility of SrPtAs with magnetic field (H) (0.35 Oe) applied along the c axis under zero-field cooling (ZFC) and field-cooling (FC) conditions is shown in Fig. 3(a). A large diamagnetic repulsion response indicates a T_c of $\sim$2.0 K as determined by the midpoint of the drop. The ZFC signal, including a demagnetization factor [29], at 1.8 K corresponds to $\sim$110% perfect diamagnetism, where $\sim$5% comes from Pb inclusions. A value greater than 100% could be due to error in the demagnetization factor estimation and/or the presence of chemical impurities. The FC curve has a slight drop that begins at $\sim$2.2 K. The lack of a large diamagnetic response could be due to nonsuperconducting impurities, vortex pinning, or a

lack of bulk superconductivity. The inset to Fig. 3(a) shows the field-dependent magnetization (M) wherein the solid red line indicates the initial slope, $4\pi \frac{dM}{dH} = -1.142$, with a corresponding superconducting volume of $\sim$110%. The lower critical field, $H_{c1} \sim 15$ Oe at 1.6 K, is estimated from the deviation of the data compared to the initial slope.

The temperature-dependent electrical resistivity, $\rho(T)$, for a SrPtAs crystal is shown in Fig. 3(b). The Pb superconducting transition at $\sim$7 K is shown in the bottom right inset. The
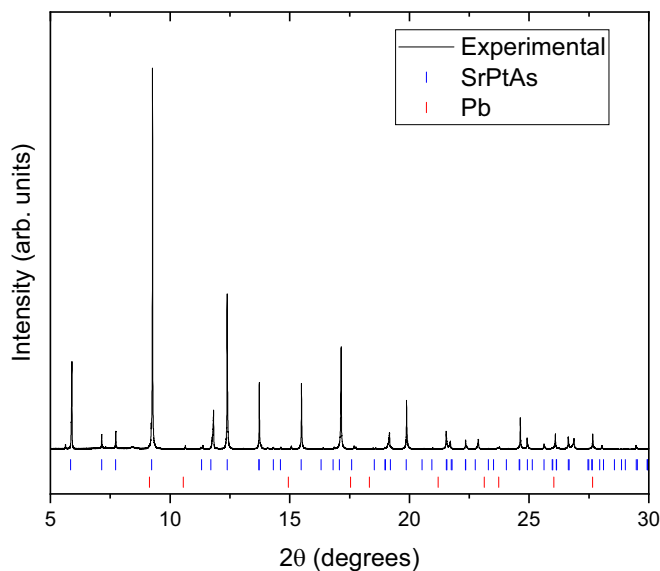

FIG. 3. (a) Temperature-dependent magnetic susceptibility [$\chi(T)$] of SrPtAs with field ($H = 0.35$ Oe) applied along the c axis. Field-cooled (FC) data are shown with red triangles and zero-field-cooled (ZFC) data are shown with black squares. Inset shows field-dependent magnetization [$M(H)$ at $T = 1.6$ K] in blue circles with the initial slope denoted with a red line. (b) Electrical resistivity [$\rho(T)$] of SrPtAs at $H = 0$. The bottom right inset shows the low temperature region (below 10 K), highlighting the superconducting transition of Pb at $\sim$7 K. The top left inset shows resistivity below 3 K where the superconducting transition of SrPtAs occurs at 2.2 K.

FIG. 2. Experimental synchrotron powder x-ray diffraction pattern for SrPtAs collected at $\lambda = 0.459$ Å under ambient conditions. Tick marks indicate Bragg peak positions for calculated SrPtAs (blue) and Pb (red) patterns. Pb impurity is less than 5%.
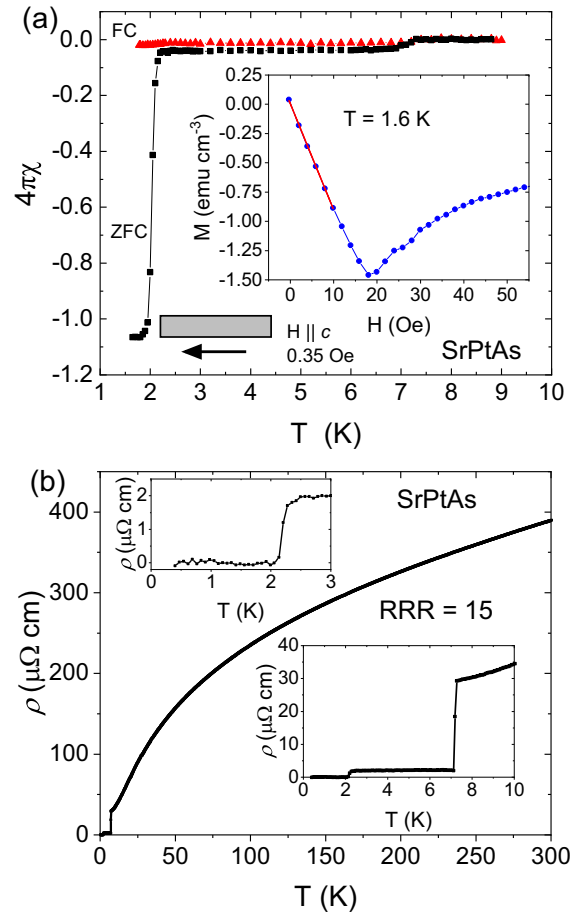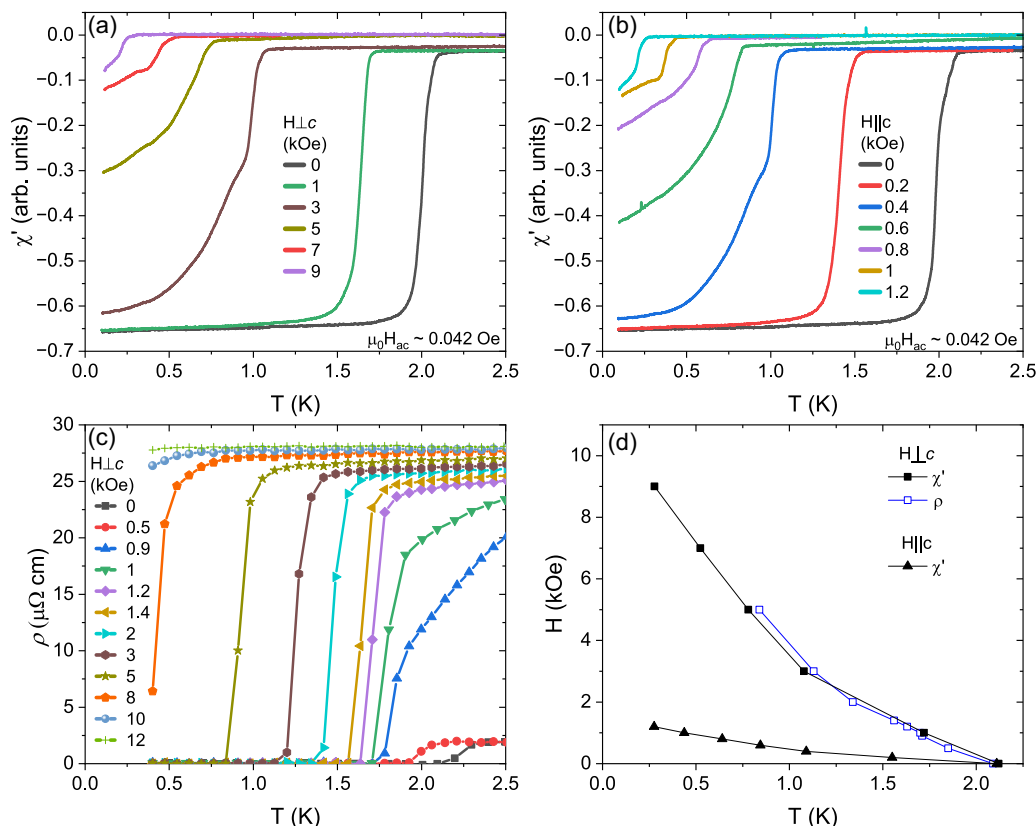
FIG. 4. (a) $\chi_{ac}(T)$ with various fields applied perpendicular to the c axis where the driving ac field ~ 0.042 Oe. (b) $\chi_{ac}(T)$ with various fields applied along the c axis where the driving ac field ~ 0.042 Oe. (c) Temperature-dependent resistivity $[\rho(T)]$ of SrPtAs with varying fields applied perpendicular to the c axis. (d) Temperature dependence of the upper critical field H_{c2}. Data determined from ac susceptibility (resistivity) measurements are shown in closed black (open blue) symbols. Data collected with field applied parallel (perpendicular) to the c axis are shown with triangles (squares).

top left inset shows a superconducting transition at 2.2 K, attributed previously to the bulk superconductivity of polycrystalline SrPtAs. Here, T_c is defined as the midpoint of the resistivity drop. The residual resistivity ratio (RRR), $\frac{\rho_{300K}-\rho_0}{\rho_0}$, is ~ 15, where ρ_0 is determined to be ~ 25 $\mu\Omega$ cm by extrapolating $\rho(T)$ from above the Pb transition at 7 K to zero temperature.

The temperature-dependent real part of the ac susceptibility (χ_{ac}), collected with various fields perpendicular and parallel to the c axis, are shown in Figs. 4(a) and 4(b), respectively. The temperature dependence of the electrical resistivity ($I||c$) at different fields perpendicular to the c axis is shown in Fig. 4(c). The upper critical field H_{c2} for both directions is shown in Fig. 4(d). T_cs for χ_{ac} were determined by the onset of each transition shown in Figs. 4(a) and 4(b). T_cs for resistivity data were determined by the point where $\rho = 0$ in Fig. 4(c). For fields parallel (perpendicular) to the c axis, the estimated upper critical field is 1.5 kOe (11 kOe). Similar extrapolations from powder samples of SrPtAs yield an upper critical field $[H_{c2(0)}]$ of 2.2 kOe [1]. Utilizing both the isotropic single-band Eliashberg model [30] and Werthamer-Helfand-Hohenberg (WHH) theory [31], $H_{c2(0)}$ was previously calculated (based on polycrystalline SrPtAs) [17]. Both values, 1.4 kOe and 1.58 kOe, respectively, agree with our linearly extrapolated lower $H_{c2(0)}$, but are significantly smaller than the $H_{c2(0)}$

perpendicular to the c axis. To calculate the WHH H_{c2} from the anisotropic data of this work, the WHH equation $H_{c2}(0) = -0.69T_c(dH_{c2}/dT)_{T_c}$ was utilized, where the resistive T_c of 2.2 K was used.

For the ac susceptibility data, the resulting $H_{c2}(0)$ for field parallel to c is 0.60 kOe and 4.4 kOe for field perpendicular to c. For the resistivity data, H_{c2} for field perpendicular to c is 3.6 kOe. Reasonably, the isotropic value determined from polycrystalline data is between the values for fields parallel and perpendicular to c. The weak BCS coupling Pauli limit $H_{c2}(0) = (1.84(T)*T_c(K))$ is determined to be 4.0 T (40 kOe) when a T_c of 2.2 K is used. When a T_c of 0.7 K is used the BCS coupling Pauli limit is 1.29 T (12.9 kOe). Both of these values exceed any estimate or extrapolation of H_{c2} for the single crystalline data.

First-principles calculations [20] obtain a quasi-two-dimensional Fermi surface with small corrugations along the c direction. Therefore, the upper critical field along this direction is significantly smaller than $H_{c2(0)}$ perpendicular to the c axis. This, coupled with the upward curvature of the upper critical field curves, could indicate that a multiband model may be applicable.

Multiple aspects of SrPtAs, such as resistivity, ac susceptibility, and the resulting upper critical field curves, are reminiscent of MgB$_2$. For example, (i) the highly anisotropic
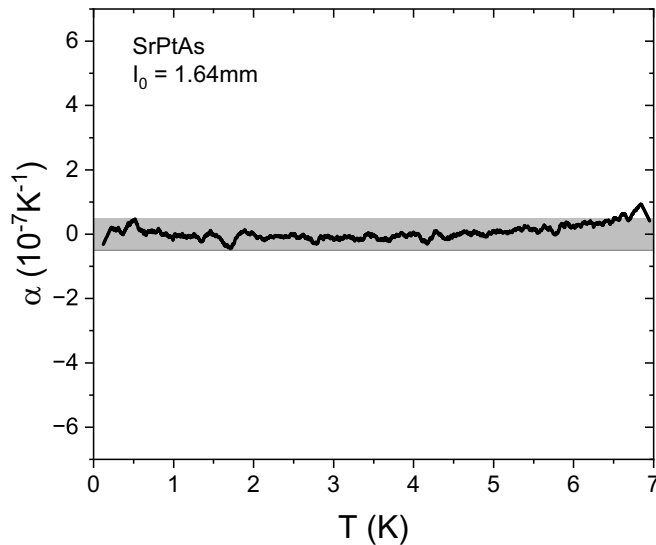
FIG. 5. Low temperature thermal expansion of SrPtAs along the c axis from 0.1 to 7 K (black line). The shaded region indicates the detection threshold of the experimental setup.
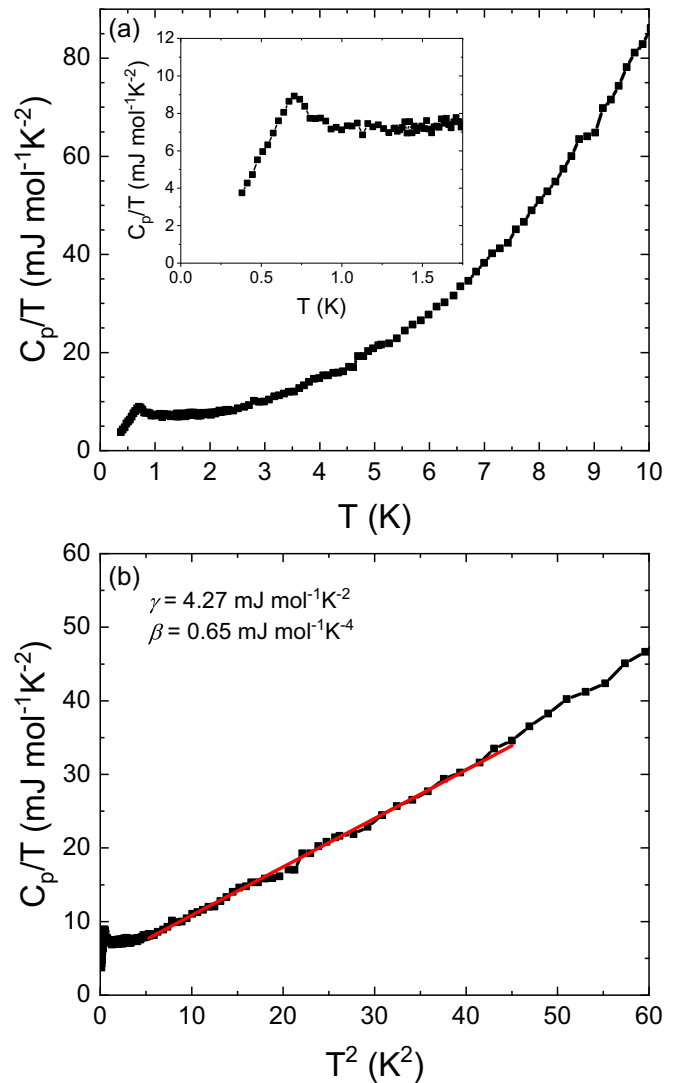

FIG. 6. (a) Heat capacity divided by temperature (C/T) shown as a function of temperature for SrPtAs. Inset shows zoomed low temperature region. (b) C_p/T as a function of T^2. The red line denotes a fit to the data of $C/T = \gamma + \beta T^2$.

nature of H_{c2} is reminiscent of MgB_2 where $H_{c2}^c \sim 2.5$ T and $H_{c2}^{ab} \sim 16$ T resulting in a low temperature anisotropy value of $H_{c2}^{ab}/H_{c2}^c = 6$–7 [32], (ii) the upward curvature of H_{c2} is an indicator of multiband superconductivity [33], and (iii) the ac susceptibility curves exhibit a kink below the onset of T_c [34] (for example, in Fig. 4(a) at 3 kOe there are two kinks, one at $\sim$1 K and one at $\sim$0.8 K) although less pronounced in the ab plane, which could indicate multiband superconductivity [32], vortex physics [32], surface superconductivity [35], or imperfect crystallinity [34]. However, the kinks have the same field dependence and anisotropy as T_c. This could indicate a change in the gap structure or vortex excitations.

Thermal expansion of the same SrPtAs crystal along the c axis, shown in black in Fig. 5, does not reveal a bulk superconducting transition. Multiple runs reveal statistical noise with no transition. The gray shaded region in Fig. 5 indicates the resolution of the experimental setup. The lack of a feature indicating a bulk superconducting transition could be because the magnitude of the transition is below the detection threshold of this experimental setup. Elemental Nb, for example, has a thermal expansion on the order of 10^{-8} K^{-1} which would not be distinguishable in this setup [36]. Additionally, SrPtAs may not have much pressure dependence of T_c along the c axis.

Heat capacity measurements were performed on the same crystal. Figure 6(a) shows specific heat divided by temperature (C_p/T) as a function of temperature. Figure 6(b) shows C_p/T as a function of temperature squared where the red line denotes the fit to the data by $C/T = \gamma + \beta T^2$. Here γ, the electronic specific heat coefficient, is 4.27 mJ/K^{2}mol and β, a constant corresponding to the Debye phonon contribution, is 0.65 mJ/K^{4}mol. The Debye temperature Θ_D is calculated from $\Theta_D = \sqrt[3]{\frac{12\pi^4 nR}{5\beta}}$ where R is the ideal gas constant (8.314 J/molK) and $n = 3$, the number of atoms per formula unit [37], yielding $\Theta_D = 208$ K. A small heat capacity jump ($\Delta C/T_c \sim 2$ mJ/K^{2}mol) is visible at 0.76 K.

Using the value of γ from the fit (= 4.27 mJ/K^{2}mol), the quantity $\Delta C/\gamma T_c = 0.47$ is obtained. Assuming a weak-coupling value of $\Delta C/\gamma T_c = 1.43$ [38], a superconducting volume fraction is estimated to be 33%. These values may be compared to $\gamma = 7.31$ mJ/K^{2}mol, $\Theta_D = 241$ K, and $\Delta C/\gamma T_c = 1.07$ for unpublished SrPtAs data mentioned in [39] and $\Delta C/\gamma T_c$ for MgB_2 of 1.09 [40].

The discrepancy between the higher T_c values ($\sim$2.0–2.4 K) determined by nonthermodynamic measurements compared to the lower T_c ($\sim$0.76 K) bulk measurements continues to be a puzzle. Possible explanations include strain-induced filamentary or surface superconductivity and/or the presence of an impurity phase. For example, in $CeIrIn_5$ resistance goes to zero at $\sim$1 K whereas specific heat data indicate bulk superconductivity at 0.4 K [41]. This discrepancy is considered to be due to strain introduced by crystallographic defects [42,43]. Other examples of filamentary or surface superconductivity include $CePt_3Si$ [44] and $WO_{2.90}$ [45].

Additional measurements, such as comparisons of multiple growth batches from various different research groups, are required to elucidate the underlying reason for the discrepancy in T_c. Because the recipe for the growth of single crystals has been determined the opportunity for additional measurements on single crystals of SrPtAs is now available.

IV. CONCLUSION

In summary, we have presented the synthesis and characterization of single crystalline SrPtAs. Magnetic susceptibility and electrical resistivity measurements show superconducting transitions at 2.0–2.4 K, consistent with previous works [1,8,15,16]. However, bulk specific heat show decreased T_c of 0.7 K. Multiple similarities between SrPtAs and MgB$_2$ have been discussed and the possibility of SrPtAs as a multiband superconductor has been considered. Our results on single crystals provide a new avenue to explore the underlying mechanisms for superconductivity in SrPtAs. Whether the difference in resistive and thermodynamic superconducting properties of SrPtAs arises from impurity phases or from strain-dependent chiral superconductivity remains an open question to be addressed by the community.

[1] Y. Nishikubo, K. Kudo, and M. Nohara, J. Phys. Soc. Jpn. **80**, 055002 (2011).

[2] M. H. Fischer, T. Neupert, C. Platt, A. P. Schnyder, W. Hanke, J. Goryo, R. Thomale, and M. Sigrist, Phys. Rev. B **89**, 020509(R) (2014).

[3] H. Ueki, S. Inagaki, R. Tamura, J. Goryo, Y. Imai, W. B. Rui, A. P. Schnyder, and M. Sigrist, Proceedings of the International Conference on Strongly Correlated Electron Systems (SCES2019) **30**, 011044 (2020).

[4] C. Kallin and J. Berlinsky, Rep. Prog. Phys. **79**, 054502 (2016).

[5] G. M. Luke, Y. Fudamoto, K. M. Kojima, M. I. Larkin, J. Merrin, B. Nachumi, Y. J. Uemura, Y. Maeno, Z. Q. Mao, Y. Mori, H. Nakamura, and M. Sigrist, Nature (London) **394**, 558 (1998).

[6] E. R. Schemm, W. J. Gannon, C. M. Wishne, W. P. Halperin, and A. Kapitulnik, Science **345**, 190 (2014).

[7] I. Kawasaki, I. Watanabe, A. Hillier, and D. Aoki, J. Phys. Soc. Jpn. **83**, 094720 (2014).

[8] P. K. Biswas, H. Luetkens, T. Neupert, T. Stürzer, C. Baines, G. Pascua, A. P. Schnyder, M. H. Fischer, J. Goryo, M. R. Lees, H. Maeter, F. Brückner, H.-H. Klauss, M. Nicklas, P. J. Baker, A. D. Hillier, M. Sigrist, A. Amato, and D. Johrendt, Phys. Rev. B **87**, 180503(R) (2013).

[9] G. Wenski and A. Mewis, Z. Anorg. Allg. Chem. **535**, 110 (1986).

[10] Y. Kamihara, H. Hiramatsu, M. Hirano, R. Kawamura, H. Yanagi, T. Kamiya, and H. Hosono, J. Am. Chem. Soc. **128**, 10012 (2006).

[11] Y. Kamihara, T. Watanabe, M. Hirano, and H. Hosono, J. Am. Chem. Soc. **130**, 3296 (2008).

[12] X. C. Wang, Q. Q. Liu, Y. X. Lv, W. B. Gao, L. X. Yang, R. C. Yu, F. Y. Li, and C. Q. Jin, Solid State Commun. **148**, 538 (2008).

[13] D. R. Parker, M. J. Pitcher, P. J. Baker, I. Franke, T. Lancaster, S. J. Blundell, and S. J. Clarke, Chem. Commun., 2189 (2009).

[14] M. Rotter, M. Tegel, and D. Johrendt, Phys. Rev. Lett. **101**, 107006 (2008).

[15] K. Matano, K. Arima, S. Maeda, Y. Nishikubo, K. Kudo, M. Nohara, and G.-q. Zheng, Phys. Rev. B **89**, 140504(R) (2014).

[16] J. F. Landaeta, S. V. Taylor, I. Bonalde, C. Rojas, Y. Nishikubo, K. Kudo, and M. Nohara, Phys. Rev. B **93**, 064504 (2016).

[17] S. Elgazzar, A. M. Strydom, and S.-L. Drechsler, J. Supercond. Novel Magn. **25**, 1795 (2012).

[18] J. Goryo, M. H. Fischer, and M. Sigrist, Phys. Rev. B **86**, 100507(R) (2012).

[19] J. Goryo, JPS Conf. Proc. **3**, 016017 (2014).

[20] S. J. Youn, M. H. Fischer, S. H. Rhim, M. Sigrist, and D. F. Agterberg, Phys. Rev. B **85**, 220505(R) (2012).

[21] M. Sigrist, D. F. Agterberg, M. H. Fischer, J. Goryo, F. Loder, S.-H. Rhim, D. Maruyama, Y. Yanase, T. Yoshida, and S. J. Youn, J. Phys. Soc. Jpn. **83**, 061014 (2014).

[22] M. H. Fischer and J. Goryo, J. Phys. Soc. Jpn. **84**, 054705 (2015).

[23] P. C. Canfield, T. Kong, U. S. Kaluarachchi, and N. H. Jo, Philos. Mag. **96**, 84 (2016).

[24] L. Krause, R. Herbst-Irmer, G. M. Sheldrick, and D. Stalke, J. Appl. Crystallogr. **48**, 3 (2015).

[25] G. M. Sheldrick, Acta Crystallogr., Sect. A **71**, 3 (2015).

[26] G. M. Sheldrick, Acta Crystallogr., Sect. C **71**, 3 (2015).

[27] Online, www.ccdc.cam.ac.uk/structures.

[28] G. M. Schmiedeshoff, A. W. Lounsbury, D. J. Luna, S. J. Tracy, A. J. Schramm, S. W. Tozer, V. F. Correa, S. T. Hannahs, T. P. Murphy, E. C. Palm, A. H. Lacerda, S. L. Bud'ko, P. C. Canfield, J. L. Smith, J. C. Lashley, and J. C. Cooley, Rev. Sci. Instrum. **77**, 123907 (2006).

[29] C. Kittel, *Introduction to Solid State Physics*, 8th ed. (Wiley, New York, 2004).

[30] J. P. Carbotte, Rev. Mod. Phys. **62**, 1027 (1990).

[31] N. R. Werthamer, E. Helfand, and P. C. Hohenberg, Phys. Rev. **147**, 295 (1966).

[32] A. K. Pradhan, M. Tokunaga, Z. X. Shi, Y. Takano, K. Togano, H. Kito, H. Ihara, and T. Tamegai, Phys. Rev. B **65**, 144513 (2002).

[33] K. H. Müller, G. Fuchs, A. Handstein, K. Nenkov, V. N. Narozhnyi, and D. Eckert, J. Alloys Compd. **322**, L10 (2001).

[34] Z. X. Shi, M. Tokunaga, T. Tamegai, Y. Takano, K. Togano, H. Kito, and H. Ihara, Phys. Rev. B **68**, 104513 (2003).

[35] U. Welp, A. Rydh, G. Karapetrov, W. K. Kwok, G. W. Crabtree, C. Marcenat, L. Paulius, T. Klein, J. Marcus, K. H. P. Kim, C. U. Jung, H.-S. Lee, B. Kang, and S.-I. Lee, Phys. Rev. B **67**, 012505 (2003).

[36] G. K. White, Cryogenics **2**, 292 (1962).

[37] N. W. Ashcroft and N. D. Mermin, *Solid State Physics* (Holt-Saunders, Philadelphia, 1976).

[38] M. Tinkham, *Introduction to Superconductivity*, 2nd ed. (Dover Publications, Mineola, 2004).

[39] K. Kudo, T. Takeuchi, H. Ota, Y. Saito, S.-y. Ayukawa, K. Fujimura, and M. Nohara, J. Phys. Soc. Jpn. **87**, 073708 (2018).

[40] H. D. Yang, J.-Y. Lin, H. H. Li, F. H. Hsu, C. J. Liu, S.-C. Li, R.-C. Yu, and C.-Q. Jin, Phys. Rev. Lett. **87**, 167003 (2001).

[41] C. Petrovic, R. Movshovich, M. Jaime, P. G. Pagliuso, M. F. Hundley, J. L. Sarrao, Z. Fisk, and J. D. Thompson, Europhys. Lett. **53**, 354 (2001).

[42] A. Bianchi, R. Movshovich, M. Jaime, J. D. Thompson, P. G. Pagliuso, and J. L. Sarrao, Phys. Rev. B **64**, 220504(R) (2001).

[43] M. D. Bachmann, G. M. Ferguson, F. Theuss, T. Meng, C. Putzke, T. Helm, K. R. Shirer, Y.-S. Li, K. A. Modic, M. Nicklas, M. König, D. Low, S. Ghosh, A. P. Mackenzie, F. Arnold, E. Hassinger, R. D. McDonald, L. E. Winter, E. D. Bauer, F. Ronning *et al.*, Science **366**, 221 (2019).

[44] K. Nakatsuji, A. Sumiyama, Y. Oda, T. Yasuda, R. Settai, and Y. Ōnuki, J. Phys. Soc. Jpn. **75**, 084717 (2006).

[45] A. Shengelaya, K. Conder, and K. A. Müller, J. Supercond. Novel Magn. **33**, 301 (2020).